River Flow Regimes From Landscape and Climate

Behnam Doulatyari[a,b,*], Andrea Betterle[c], Stefano Basso[a,b], Basudev Biswal[d], Mario Schirmer[a,b], Gianluca Botter[c]

[a] *EAWAG (Swiss Federal Institute of Aquatic Science and Technology), Department of Water Resources and Drinking Water, Duebendorf, Switzerland*
[b] *University of Neuchtel, The Centre of Hydrogeology and Geothermics (CHYN), Neuchtel, Switzerland*
[c] *University of Padova, Department ICEA and International Center for Hydrology "Dino Tonini", Padua, Italy.*
[d] *Indian Institute of Technology Hyderabad, Department of Civil Engineering, Hyderabad, India*

Abstract

Characterizing the probability distribution of streamflows in catchments lacking in discharge measurements represents an attractive prospect with consequences for practical and scientific applications, in particular water resources management. In this paper, a physically-based analytic model of streamflow dynamics is combined with existing water balance models and a geomorphological flow recession model in order to estimate streamflow probability distributions based on catchment-scale climatic and morphologic features. Starting from rainfall data, potential evapotranspiration and digital terrain maps, the model proved capable of capturing the statistics of observed streamflows reasonably well in eleven test catchments (Mean Squared Relative Error equal to 0.13 and 0.06 for the mean discharge and coefficient of variation of daily flows respectively). The approach developed offers a novel method for estimating water resources availability based on limited information about climate and landscape.

Keywords: streamflows, stochastic model, flow duration curve, physically-based

1. Introduction

The probability distribution of streamflows and the associated flow duration curve provide information on the availability of water resources in a catchment. This is important both for anthropogenic exploitation of flows (e.g. industrial and civil uses or

*Corresponding author
Email address: behnam.doulatyari@eawag.ch (Behnam Doulatyari)

power generation) and the maintenance of functioning ecological processes within the riverine environment [*Postel and Richter,* 2003; *Ziva et al.,* 2012; *Hurford et al.,* 2014;]. Streamflow probability distributions summarize main features of the flow regime, as well as flow dynamics related to different geographical and climatic settings. For this reason, they have long been a key tool for water resource management [*Vogel and Fennessey,* 1995].

The absence of dense discharge measurement networks makes the assessment of river flow availability challenging. Extensive literature exists on estimation of flow duration curves in sparsely gauged and ungauged catchments [*Merz and Blöschl,* 2004; *Blöschl et al.,* 2006; *Castellarin et al.,* 2004; *Oudin et al,* 2008; *Castiglioni et al.,* 2010; *Hrachowitz et al.,* 2013]. Both empirically-based and physically-based approaches are suited to the scope. Among the former, statistical models employ discharge time series observed at instrumented outlets of neighboring catchments or within identified homogeneous regions to predict the flow regime of ungauged basins using the concept of hydrologic similarity [*Wagener and Wheater,* 2006; *Castellarin et al.,* 2007; *Ganora et al.,* 2009]. Physically-based approaches, instead, mimic the hydrologic response of the basin to rainfall inputs by describing the underlying processes of soil moisture dynamics and rainfall-runoff transformation [*Beven and Kirkby,* 1979; *Botter et al.,* 2007; *Yokoo and Sivapalan,* 2011; *Cheng et al.,* 2012; *Booker and Woods,* 2014]. Such models have the advantage of setting causal relationships among climate input, morphological features, and geopedologic attributes allowing for an improved understanding of the physical processes that control the water cycle [*Wagener et al,* 2007; *Gupta et al.,* 2008; *Hrachowitz et al.,* 2013].

Many studies have highlighted the relationship between channel network structure and hydrologic response of the catchment [*Rinaldo,* 1991; *Rinaldo et al.,* 1995; *Rodriguez-Iturbe et al.,* 2009; *Biswal and Marani,* 2010; *Mutzner et al.,* 2013; *Gosey and Kirchner,* 2014]. In particular, geomorphological interpretations of recession dynamics have been proposed, which have been used to infer geomorphic signatures of the hydrologic response [*Harman et al.,* 2009; *Biswal and Marani* 2014]. Given the wide availability of high resolution Digital Elevation Models (DEM), the link between geomorphological attributes of the landscape and flow properties is particularly interesting for improving our ability to describe flow regimes in poorly gauged areas.

Landscape properties and catchment morphology have also been recognized as major determinants of vegetation patterns, water use efficiency and hydrologic partitioning [*Troch et al.,* 2009; *Rodriguez-Iturbe et al.,* 2009; *Voepel et al.,* 2011; *Thompson et al.,* 2011a]. The understanding of the major drivers of the water balance has a long history, which is rooted in pioneering works by *Thornwaite* [1948], *Longbein* [1949] and *Budyko* [1974] who first demonstrated the dependence of hydrologic partitioning on climate features, as well as on the competition between available soil water and available energy for vaporization. More recent works have highlighted that the seasonality and stochasticity of rainfall, vegetation features, and landscape properties are also important for attaining reliable predictions of water balance [*Milly,* 1994; *Porporato et al.,* 2004; *Donohue et al.,* 2007; *Zhang et al.,* 2008]. Despite the inherent difficulty in incorporating the effects of soil, vegetation and climate heterogeneity into low dimensional catchment-scale formulations, our understanding of the spatio-temporal variability of hydrologic partitioning between streamflow and evapotranspiration has improved significantly in recent years [*Sivapalan et al.,* 2001; *Thompson et al.,* 2011b; *Zanardo et al.,* 2012]. These advances can provide important clues for the prediction of water resources in rivers and for forecasting of their response to climate change [*Destouni et al.,* 2013].

In this study, we present and exemplify a physically-based framework capable of predicting the flow regime in the absence of discharge data. The framework is grounded in the stochastic analytic model developed by *Botter et al.* [2007]. This is a mechanistic approach where the dynamics of daily streamflows are linked to a spatially-integrated soil water balance forced by intermittent rainfall. This paper adopts the version of the model in which the hydrologic response of the catchment is assumed to be non-linear [*Botter et al.,* 2009; *Ceola et al.,* 2010]. The four physically-based parameters that define the flow duration curve are estimated based on climatic (rainfall and potential evapotranspiration) and geomorphological data (Digital Elevation Maps), integrating established water balance models [*Budyko,* 1974; *Milly,* 1994; *Porporato et al.,* 2004; *Sivapalan et al.,* 2011] with a geomorphic recession flow model [*Biswal and Marani,* 2010]. The framework is meant to mimic conditions that are typical of sparsely gauged areas and exploit a set of gauged catchments and a lumped regional approach for estimating the water balance based on climate data. Moreover, the model explicitly incorporates

the geomorphic relationship between the river network structure and recession properties of flows.

This paper is organized as follows: section 2 provides a summary of the hydro-climatic data, the selection criteria for the study catchments, and the essential information about these catchments. In section 3, we introduce the analytical model for the probability density function of streamflows and define the relevant model parameters. Section 4 outlines the method proposed for the parameter estimation in the absence of discharge data. In particular, the performance of different water balance models were tested for the estimation of the frequency of flow producing events. The ranking of the water balance models and the results of predicting the streamflow regimes are discussed in section 5. In this section the limitation of the proposed framework are elaborated on. Section 6 provides the overall conclusions of this study.

2. Study Catchments and Hydro-climatic Data

49 catchments were used in this study in two sets: (i) catchments used for calibration of the water balance model (Table 1); (ii) catchments were streamflow distribution was predicated using only climate data (calculated based on the calibrated water balance model) and morphological data (Table 2). The catchments are distributed relatively evenly throughout the United States, east of the Rocky Mountains. The size of the basins span between 40 and 2000 km^2 and include many different climatic regions. All the study catchments are pristine and not impacted by regulation or storage. Figure 1 shows the spatial distribution of the 49 catchments across the US. The $CGIAR$ average annual potential evapotranspiration is shown on the background to represent the underlying heterogeneity of climate regimes. The northern catchments (marked with a dotted circle) experience relevant snow precipitations during winter. The presence of snow significantly impacts the water balance across seasons, in particular by storing water inside the catchment in winter (when precipitation occurs) and releasing the stored water in spring (when the snow melting increases the runoff coefficient). Thus, in the catchments affected by snow dynamics, results from winter and spring were disregarded in the application of water balance models at the seasonal scale.

Potential Evapotranspiration (PET) data has been acquired through two different

data bases: (*i*) The 'MODIS global evapotranspiration Project' (MOD16), available from the Montana University (`http://www.ntsg.umt.edu`), which includes a dataset providing PET at 1 km^2 resolution for 10^9 Million km^2 global vegetated land areas at 8-day, monthly and annual time resolution; (*ii*) The 'CGIAR-CSI Global-Aridity and Global-PET Database' [*Zomer et al.,* 2007], a freely available global PET database (`http://www.cgiar-csi.org`). This information was integrated into a geographical information system (ESRI ArcGis 10.0). The exact location of the discharge gauges were determined on a detailed map of the river network of the United States provided by the NOAA (info: `http://www.nws.noaa.gov/geodata/catalog/hydro/metadata/riversub.htm`; download: `https://www.ncl.ucar.edu/Applications/Data/`). The contributing catchments and drainage networks upstream of the discharge gauging stations were then estimated.

Daily rainfall records provided by the American National Oceanic and Atmospheric Administration (NOAA), and daily discharge records provided by the United States Geological Survey (USGS) were used in this study. Available time series typically span several decades. A set of pristine catchments, where synchronous rainfall and discharge data were available for at least 10 years, was selected. For each streamflow gauging station selected in the study, a representative rainfall station (located as close as possible to the center of the catchment area) was selected. The reliability of using just one rainfall gauge for each catchment was supported by previous studies [see *Botter et al.,* 2013], which proved that given the size of the basins (Table 1) selected in this study, the spatial variability of daily rainfall statistics is weak, and the use of a single rainfall station does not introduce any remarkable bias in the analysis. Finally, spatially averaged value of PET was calculated for every catchment and every PET dataset.

3. Analytical Model of p(Q): Linking Flow Regime to Geomorphoclimatic Data

The river flow regime can be captured and presented through the seasonal probability density function (PDF) of daily streamflows. In this work, we employ the analytical mechanistic model developed by *Botter et al.* [2009]. This model is based on a catchment-scale soil water balance forced by stochastic rainfall which is modeled (at daily timescales)

as a marked Poisson process with frequency $\lambda_P[T^{-1}]$ and exponentially distributed depths with average $\alpha[L]$ [*Rodriguez-Iturbe et al.,* 1999; *Porporato et al.,* 2004; *Botter et al.,* 2007]. In this framework the dynamics of the specific streamflow Q (per unit catchment area) is made up of two components: (i) instantaneous jumps corresponding to rainfall events filling the soil water deficit in the root zone. These events take place with frequency $\lambda < \lambda_P$ and are also represented by a marked Poisson process; (ii) power law decays in between events as implied by a non-linear catchment-scale storage-discharge relationship [*Brutsaert and Nieber* 1997; *Porporato and Ridolfi,* 2003; *Kirchner,* 2009; *Ceola et al.,* 2010]. Therefore, the temporal dynamics of Q during a given season is described by the following relation:

$$\frac{dQ\,(t)}{dt} = -KQ\,(t)^a + \xi_Q(t) \tag{1}$$

where $\xi_Q(t)$ represents the stochastic noise (the sequence of state dependent random jumps of Q, associated with those rainfall events which produce streamflow); $K[L^{1-\alpha}T^{\alpha-2}]$ and a are the coefficient and exponent of the power law relation that describes the rate of decrease of Q during the recession. The steady-state PDF of streamflows can be derived from the solution of the master equation associated to equation (1) [*Botter et al.,* 2009] as:

$$p(Q) = CQ^{-a} \exp\left(-\frac{Q^{2-a}}{\alpha K(2-a)} + \frac{\lambda Q^{1-a}}{K(1-a)}\right) \tag{2}$$

where C is a suitable normalizing constant. Equation (2) expresses the seasonal flow regime as a function of four physically-based parameters that embed the geomorphic and climate features of the contributing catchment. The original formulation (see eq.(2) of *Ceola et al.* [2010]) includes an atom of probability for $Q = 0$ for cases where $0 < a < 1$. Such conditions are rare in real world settings [*Biswal and Marani,* 2010; *Ceola et al.,* 2010; *Mutzner et al.,* 2013] and thus only cases with $a > 1$ have been considered in this study.

The flow duration curve is expressed by the cumulative distribution function (CDF) of Q and can therefore be calculated by integrating equation (2):

$$D(Q) = \int_Q^{+\infty} p(x)dx \tag{3}$$

Closed-form analytical expressions of $D(Q)$ are available only for special cases (e.g. $a \in \mathbb{N}$). The above model considers streamflows at the daily time scale and fast com-

ponents of the hydrologic response are implicitly incorporated in the non-linear storage-discharge relationship that drives the soil drainage. The major assumptions underlying the analytical formulation shown in equation (2) are: (*i*) the Poisson distribution of flow-producing events; (*ii*) the exponential distribution of the daily rainfall (and effective rainfall) depths; (*iii*) the lack of inter-event variability of recession features; (*iv*) the spatial homogeneity of climate and landscape properties. Moreover, the interference caused by snow accumulation and melting is not explicitly included in the formulation. Extensive applications and generalizations of this approach have been published in previous studies [*Botter et al.,* 2010, 2013; *Ceola et al.,* 2010; *Pumo et al.,* 2013; *Schaefli et al.,* 2013; *Mejia et al.,* 2013; *Müller et al.,* 2014].

4. Estimating the Parameters of p(Q)

The PDF of streamflows (equation (2)) relies on four parameters: α, λ, K, and a, which incorporate important climatic and geomorphologic features of the catchment. The value of α is estimated using climate data gathered within each test catchment. a and K are estimated for each test catchment through a geomorphic recession model that is applied locally. The value of λ is estimated for each test catchment through water balance models that are independently calibrated based on discharge data from 38 different catchments distributed east of the rocky mountains in the US. These methods are explained in detail below.

4.1. Computation of α

Mean rainfall depth (α) is estimated by means of daily rainfall data recorded at climatic stations within the boundaries of each catchment. In particular, α is calculated as the mean precipitation during wet days in the considered season.

4.2. Computation of λ

According to the analytical formulation (equation (1) and (2)) the long-term mean of Q is defined as $< Q >= \alpha\lambda$. Therefore, the frequency of effective rainfall events λ is estimated from precipitation using a water balance model as $\lambda = \phi\, \lambda_p$, where λ_p is the frequency of rainfall events (estimated as the relative fraction of rainy days in the

seasonal time series) and $\phi =< Q > / < P >$ is the average seasonal runoff coefficient (i.e. the ratio of mean discharge to mean precipitation). ϕ can be estimated by means of calibrated water balance models using precipitation and PET data.

Four existing water balance models were tested and compared by analyzing their ability to predict observed runoff coefficients at 38 catchments within the study region (Table 1). This number was deliberately maximized to test each model under a broad range of hydro-climatic conditions and identify the best approach in general within the study area. The models include empirical, semi-empirical and physically-based approaches (Table 3 and reference therein). Each model has a different number of parameters, which were calibrated in order to maximize model performances. We assume the spatial variability of the water balance within the study region can be explained by the underlying heterogeneity of the precipitation and PET. Hence, model parameters were assumed to be spatially homogeneous, so that the calibrated parameters can be exported to other catchments within the study region, including the eleven test catchments where flow regimes are predicted.

The first model (WB1) represents the widely accepted empirical Budyko curve [*Budyko, 1974*]. The Budyko curve represents a very simple and effective way to estimate the annual runoff coefficient, based on rainfall and PET data. The runoff coefficient is estimated as a non-linear function of the 'Dryness Index' (D_I), defined as the ratio between annual average potential evapotranspiration and the annual average rainfall ($\langle PET \rangle / \langle P \rangle$). The analytical function of the Budyko curve reads:

$$\phi = 1 - \left[D_I (1 - e^{-D_I}) \, tanh \left(\frac{1}{D_I} \right) \right]^{0.5} \tag{4}$$

In this model the only variable involved is D_I, which depends on rainfall and potential evapotranspiration. In our application rainfall is measured in climatic stations and the PET is derived from either the $MODIS$ or the $CGIAR$ dataset. Therefore, there are no parameters to be calibrated.

The second model (WB2) is a physically-based minimalist model, where the catchment water-storage is seen as a stochastic state variable that governs the water balance either point-wise [*Rodriguez-Iturbe et al.,* 2001] or at the catchment scale [*Porporato et al.,* 2004; *Seltin et al.,* 2007]. Soil moisture dynamics are interpreted and modeled at

daily time scales, by conceptualizing the soil as a reservoir with a finite storage capacity (equal to nZ, where n is porosity and Z the rooting depth) intermittently filled by rainfall events in the form of random pulses with random depth. When soil moisture s exceeds a given threshold s_1 (an empirical parameter with a value between field capacity and complete saturation), the excess rainfall is lost by vertical drainage. Water losses occur via evapotranspiration (which is smaller than PET for $s < s_1$ due to water stress), drainage and surface runoff (when the soil is saturated). The mean runoff coefficient is written as [*Porporato et al.,* 2004]:

$$\phi = \frac{D_I \gamma^{\frac{\gamma}{D_I}} e^{-\gamma}}{\gamma \left(\Gamma(\gamma/D_I, \gamma)\right)} \tag{5}$$

where, $\Gamma(\cdot, \cdot)$ is the lower incomplete Gamma function, D_I is the Budyko's dryness index, and γ the maximum soil water storage available to plants normalized to the mean rainfall depth ($\gamma = \frac{(s_1 - s_w)nZ}{\alpha}$, with s_w representing the wilting point). D_I is calculated from climatic data. Consequently, calibration was performed on the rooting depth. This model is particularly suited to be used in association with the streamflow model used in this paper, which was originally conceived by coupling WB2 with a simplified hydrologic response model [*Botter et al.,* 2007].

The third model (WB3) [*Milly,* 1994] is based on the hypothesis that the long-term water balance is determined by the local interaction of fluctuating water supply (precipitation) and demand (potential evapotranspiration), mediated by water storage in the soil. The partitioning of average annual precipitation into evapotranspiration and runoff is assumed to depend on the following factors: dryness index, the mean number of precipitation events per year, the ratio of spatially averaged soil water holding capacity to the annual average precipitation, the spatial variability of storage capacity, and seasonality of precipitation and PET. The model postulates that in humid areas ($D_I < 1$) the dominant factor producing runoff is the excess of annual precipitation over annual potential evapotranspiration; in arid regions ($D_I > 1$), instead, runoff is largely caused by forcing variability over time. The resulting analytical expression of the runoff coefficient reads

[*Milly,* 1994]:

$$\phi = 1 - (1 - D_I) \sum_{j=0}^{\infty} \left[1 + j\gamma(D_I^{-1} - 1)k^{-1}\right]^{-k} {D_I}^j \qquad \texttt{for} \qquad D_I < 1 \quad (6)$$

$$\phi = 1 - (1 - D_I^{-1}) \sum_{j=0}^{\infty} \left[1 + (j+1)\gamma(1 - D_I^{-1})k^{-1}\right]^{-k} {D_I}^{-j} \qquad \texttt{for} \qquad D_I > 1 \quad (7)$$

where γ represents the normalized soil water storage and D_I is the dryness index. Spatial heterogeneity of soil properties is accounted for through the shape parameter k of the Gamma PDF that describes the spatial distribution of soil storage capacity. In WB3 the calibrated parameters were Z and k.

Model WB4 [*L'vovich,* 1979; *Ponce and Shetty,* 1995a, 1995b; *Sivapalan et al.,* 2011] is an annual water balance which is performed through a two-stage partitioning: first, annual precipitation P is decomposed into quick flow (S) and infiltration (termed catchment wetting, W). Subsequently, the resulting wetting is partitioned into slow flow (U) and an energy-dependent vaporization component (evaporation plus transpiration ET). This two-stages portioning can be written as $P = S + W$ and $W = U + ET$. The threshold values of P and W that must be exceeded before flow can occur are defined as $\lambda_s W_p$ and $\lambda_u PET$ respectively, where λ_s and λ_u are empirical parameters. W_p and PET are the upper bounds of $\langle W \rangle$ and $\langle ET \rangle$, which thus represent the potential wetting and the potential evapotranspiration of a catchment, respectively. Both the quick-flow and slow-flow components need to be combined to yield the total discharge in the stream ($Q = U + S$). The runoff equation is then expressed as [*Sivapalan et al.,* 2011]:

$$\phi = \frac{1 + \widetilde{\langle P \rangle}\varphi}{1 + \varphi + \widetilde{\langle P \rangle}\varphi} \quad (8)$$

where, $\varphi = \frac{PET - \lambda_u PET}{\langle P \rangle - \lambda_s W_p}$ and $\widetilde{\langle P \rangle} = \frac{\langle P \rangle - \lambda_s W_p}{(1 - \lambda_s) W_p}$.

This model was calibrated in different ways. Initially the 4 parameters ($\lambda_s, \lambda_u, W_p, PET$) were calibrated as in the original version of the model. Subsequently, in order to preserve the spatial variability of evapotranspiration, the available estimate of PET provided by the $MODIS$ and $CGIAR$ datasets (multiplied by a calibrated correction factor ξ) was included in the model formulation. Finally, with the goal of keeping the model viable for application in catchments where discharge measurements are lacking, the partitioning of P into S and W (whose application requires discharge data) was removed, thereby

implying that all precipitation is turned into soil wetting. In this way the number of parameters to be calibrated is reduced to just one (λ_u). Given that the latter version of the model maximizes model performance across the 38 study catchments, this is the calibration method applied to WB4 as discussed in the results section.

Some of the models presented above are based on hypotheses that only hold at the annual time-scale (WB3), or they have been previously applied mainly at the annual level (WB1). Because of this reason they are best applicable to estimate annual runoff coefficients. To get an estimate of the inter-seasonal variability of streamflow regimes during the year, the knowledge of seasonal average runoff coefficients would instead be desirable. To this aim, a novel approach has been developed in order to describe the inter-seasonal variability of the water balance based on annual estimates.

The average annual runoff coefficient ($\phi_a = \frac{\langle Q \rangle_a}{\langle P \rangle_a}$) can be expressed as a weighted mean of the seasonal average runoff coefficients. Accordingly, the seasonal runoff coefficient $\phi_i = \frac{\langle Q \rangle_i}{\langle P \rangle_i}$ can be calculated by multiplying the annual runoff coefficient ϕ_a by a Seasonal Multiplication Factor ψ_i which expresses the inherent seasonality of the water balance:

$$\phi_i = \phi_a \psi_i \tag{9}$$

where ϕ_a is estimated using one of the four water balance models described above, and $\psi_i = \phi_i / \phi_a$ is the ratio between seasonal and annual runoff coefficient during the season i. Note that the typical subdivision into four seasons, broadly following the calendar dates, has been adopted in this paper. Equation (9) expresses the idea that even though the annual runoff coefficient may vary significantly among catchments, the seasonal pattern may be relatively uniform across a wide range of conditions. Despite some scattering, the results obtained in the 38 study catchments corroborate the assumption that ψ_i are quite homogenous (see Figure 2). The values of ψ_i were thus assumed to be spatially uniform and were calibrated based on observed rainfall and streamflow data.

4.3. Computation of a and K

The estimation procedure for the recession parameters a and K is rooted in the idea that recession properties are strongly related to the morphology of the stream network [*Biswal and Marani,* 2010; *Biswal and Nagesh Kumar,* 2014; *Mutzner et al.,* 2013; *Biswal*

and Marani, 2014]. During recessions both the streamflow and the active drainage network – which represents the fraction of the network that actively contributes to the flow at the outlet – decrease over time [*Gregory and Walling,* 1968; *Weyman,* 1970; *Godsey and Kirchner,* 2014]. The active drainage network (ADN hereafter) is thus assumed to expand and contract following the related streamflow fluctuations. The theoretical apparatus on which the method is grounded, as well as the performance of the model under various settings are detailed in a series of recent papers about the geomorphic nature of flow recessions [*Biswal and Kumar* 2013; *Biswal and Marani,* 2014 and references therein], where the relevant details can be found. In summary, the specific streamflow Q is expressed as:

$$Q = \frac{q\,G}{A} \tag{10}$$

where G is the length of the active drainage network, q is the flow generation rate per unit channel length, and A the catchment area. Three simplifying assumptions are then introduced:

- drainage density is spatially uniform;
- both the flow generation per unit channel length q and the speed at which the ADN contracts towards the outlet (c) are constant;
- the changes of G through time are expressed in terms of the changes of G induced by changes of the maximum path length within the ADN, l (which is the maximum distance between a point of ADN and the furthest source of the network): $dG/dt = dG/dl \cdot dl/dt = c\,dG(l)/dl$.

Under these assumptions, the recession equation $dQ/dt = KQ^a$ can be rewritten as [*Biswal and Marani,* 2014]:

$$\frac{N(l)}{A} = \rho' \left(\frac{G(l)}{A} \right)^a \tag{11}$$

where $N(l) = dG(l)/dl$ is the number of links in the network at a distance l from the outlet, and $\rho' = Kq^{a-1}/c$. Equation (11) states that the recession exponent a can be estimated from the morphology of the basin by analyzing the scaling exponent of the geomorphic relationship between $N(l)$ and $G(l)$, as shown in Figure 3. These functions can be derived from the analysis of digital terrain maps, thereby allowing an objective

estimate of the recession exponent from morphological data. This is in turn used for the computation of the scaling exponent of the functions $G(l)$ vs. $N(l)$ through leas-squared regression.

In order to estimate the recession coefficient K, we first calculate the temporal mean of Equation (10):

$$\langle Q \rangle = \frac{q \ \langle G \rangle}{A} = q \, D_d \tag{12}$$

which expresses the mean discharge $\langle Q \rangle$ as the product between the mean drainage density ($D_d =< G > /A$) and flow generation rate per unit channel length (q). Next, Equation (12) is equated to the analytical expression of mean specific discharge ($\langle Q \rangle = \alpha\lambda$) provided by the streamflow model. q can then be expressed as:

$$q = \frac{\alpha\lambda}{D_d} \tag{13}$$

Combining the definition of ρ', mentioned before, with Equation (13) leads to:

$$K = \rho' c q^{a-1} = \theta(\alpha\lambda)^{1-a} \tag{14}$$

where $\theta = \rho' c / D_d^{1-a}$. Equation (14) expresses that K is inversely related to the mean humidity conditions of the contributing catchment (quantified here through $\alpha\lambda$), as well as to the recession exponent a. Empirical analysis based on observed recessions in multiple catchments suggests that the value of θ is fairly constant across different catchments and seasons. Therefore, here we assume θ to be constant and calculate its value based on summer season streamflows in a randomly selected pilot catchment (Williams Basin, US where $\theta = 0.23 \, d^{-1}$). Equation (14) can then be used to predict K based on a, α and λ. The analytical expression for streamflow PDFs (Equation (2)) is poorly sensitive to the value of K [see *Botter et al.,* 2009]. Therefore, a more accurate method for estimation of K is deemed not necessary in this context.

In the eleven test catchments where the prediction of flow regime was performed, the river network was estimated based on 30 m USGS DEMs (obtained from: http://gdex.cr.usgs.gov/gdex/). These catchments can be broadly classified as gently sloping (average slope $<$ 5%). Therein, the D8 flow direction algorithm [*Mark*, 1988] was used to obtain the flow direction maps, and subsequently, the flow accumulation maps. Flow accumulation threshold of $0.09 \, km^2$ was then imposed to delineate channel networks for these eleven test catchments.

5. Results and Discussion

5.1. Water Balance Model Ranking

For the presentation of the results of water balance models, the following notation has been used to uniquely identify each model and the set of possible variants adopted. Each water balance model is labeled by a string which is composed of four parts:

$$\underbrace{\mathbf{WB1}}_{1}.\underbrace{\mathbf{ET1}}_{2}.\underbrace{\mathbf{A}}_{3}\underbrace{\mathbf{(1)}}_{4}$$

(1) refers to the specific water balance model (Table 3); (2) identifies the potential evapotranspiration dataset used in the model calibration: ET1 refers to $CGIAR$ while ET2 refers to $MODIS$; (3) denotes the model time scale: A implies the model has been applied at the annual time scale; S implies the model has been applied at the seasonal time scale; Sc implies that the model has been applied at the annual time scale and then the seasonal water balance has been evaluated by making use of the seasonal multiplication factors ψ; (4) specifies the numbers of model parameters used in the calibration (when necessary).

Many of the models considered include the average rooting depth Z as a key parameter. Z drives the maximum soil moisture storage capacity $nZ(s_1 - s_w)$. Hence, for convenience and without any loss of generality, s_w, s_1 and n are assumed to be constant throughout all simulations (and equal to 0.2, 0.5 and 0.35, respectively), while only Z was calibrated. Note that different versions of each model were implemented, where either a single value of Z or different values of Z for each season were considered.

With regards to the four water balance models, the deviance of observed vs. modeled results is quantified by the Mean Square Error (MSE), defined as $MSE = 1/N \sum_{i=1}^{N} \epsilon_i^2$ where ϵ is the difference between modeled and observed runoff coefficients, and N is the number of cases in which the models are tested. Furthermore, performances of each model has been objectively quantified by means of the *Akaike Information Criterion* (AIC) [*Akaike,* 1973]. The method provides a rigorous way for model selection based on the maximization of the log-likelihood function between experimental data and model estimates. The goodness of fit of each model is discounted by accounting for the number of parameters that are fitted to observations. The formulation of AIC used to rank the

different water balance models in this study is as follows:

$$AIC = 2\,N\,MSE + 2(M+1), \tag{15}$$

where N is the number of independent observations used to evaluate the models and M is the number of calibrated parameters. Table 4 summarizes the performances of the water balance models applied at the annual time scale and values of calibrated parameters that optimize model performance.

WB1 and WB2 prove quite effective at the annual timescale, especially in association with ET1. Overall, WB4 seems to be the best model in order to estimate the average annual water balance in the study area. Though, its performance is only slightly better than those of WB1 which has no calibrated parameters. It is noteworthy to mention that the calibration of the annual models led to reasonable values of Z in all cases ($500 < Z < 1000$), in agreement with previous studies [*Allen et al., 1998*]. In general all models perform better when coupled with the ET1 dataset.

Table 5 summarizes the results of the water balance models applied at the seasonal time scale. The performance of WB1 at seasonal scale is not as good as those at annual time scale. Even though the absence of parameters is an appealing feature of the Budyko approach, WB1 does not seem robust enough to estimate the seasonal water balance in the study catchments. The overall performance of the method utilizing annual models and the seasonal multiplication factors are comparable (if not superior) to the performance of the same models applied directly at the seasonal timescale. In fact, the observed inter-catchment variability of ψ_i across the study area (in the set of 38 calibration catchments) is relativity low (Figure 2) despite the broad range of hydro-climatic conditions explored. When the seasonal multiplication factors are used, the best performing models are WB2 and WB3. Overall, at seasonal time scale, WB2 was found to be the best performing model, achieving better performances than all other models, especially when the rooting depths Z was separately calibrated for each season.

The plots in Figure 4 show the scatter-plot of a select number of calibrated models (including the three best performing models) at the seasonal time scale for the 38 calibration catchments. On the y-axis the modeled value of the runoff coefficient is shown, while the observed value, calculated as the ratio between the average seasonal precipitation and runoff, is shown on the x-axis. Despite some scattering, WB1 and WB2 (presented here)

exhibit satisfying performances and do not show any systematic biases in estimating the seasonal runoff coefficients.

The performances of all four models at the seasonal time scale, without differentiation between the two PET datasets and the different versions of each model implemented, are shown in Figure 5. The histograms represent the frequency distribution of ΔAIC among the variants of each model and are complemented with the median value of ΔAIC, thereby allowing an objective assessment of the overall performances of each approach. The histograms highlight how WB2.ET2.S(4) is characterized by the smallest mean value of ΔAIC, implying that (on average) it outperforms the other models.

Lastly, WB2.ET2.S(4) was utilized for predicting the runoff coefficient at 11 test catchments. The ability of WB2.ET2.S(4) to describe the seasonal water balance at the eleven test catchments is analyzed in Figure 6, which compares observed vs. estimated values of the runoff coefficient for all the available seasons. Performance is relatively good in most cases, especially in view of the fact that no specific information on observed discharge at the test catchments has been used.

5.2. Prediction of $p(Q)$

Streamflow distributions for every season were predicted at 11 catchments, corresponding to 44 seasonal regimes (Table 2). The catchments are basins with natural streamflows, not affected by regulation or significant snow dynamics, and are distributed across the study region. It is important to note, this study is aimed at presenting and exemplifying the general methodology, and therefore, large-scale application is beyond the scope of the paper.

The parameters of the analytical streamflow PDF were estimated for the eleven test catchments using only climate and landscape data as discussed in Section 4. Table 6 shows the resulting values of α, λ, a and K for each season in the eleven test catchments. For comparison, the observed values of λ, a and K were also calculated based on discharge data [*Biswal and Marani,* 2010; *Ceola et al.,* 2010]. The geomorphological estimates of a (which are assumed to be independent of season) show a general agreement with the median value of the recession exponent calculated based on discharge data with the exception of a moderate discrepancy that emerges during summer seasons. Similarly, the estimates of λ based on precipitation and PET data show a broad agreement with the

corresponding estimates based on discharge data. The geomorphological estimates of K instead, are in agreement only in half the cases when compared to the estimated value of the recession coefficient based on discharge observation. It is important to note that the value of θ is relatively constant across different catchments and seasons in the catchments considered here ($CV \approx 0.2$), thereby corroborating the reliability of the assumption that θ is constant in Equation (14).

Equation (2) is used to model the "period-of-record" PDF and CDF curves in the eleven test catchments. The agreement between modeled and observed PDFs (and the associated CDFs) was evaluated through visual inspection, comparison of modeled and observed moments of the PDF, and objectively quantified by computing half the integral difference between the analytical and observed flow PDFs [*Botter et al.,* 2013]. The accuracy of the model is further analyzed by the Mean Squared Relative Error (MSRE) of selected flow statistics (see Table 1 in [*Biondi et al.,* 2012]).

Figure 7 presents the observed (bars) and modeled (solid line) seasonal streamflow PDFs at Daddy creek, US. The analytical model captures the shape of the observed probability distribution of flows relatively well in all seasons. Though, the model seems to slightly underestimate the high flows, providing lower probability for large events as compared to the observations. The ability of the model to catch the change in shape of the streamflow distribution across different seasons is particularly valuable. On a seasonal time scale, a catchment can produce both erratic and persistent regimes [*Botter et al.,* 2013]. In persistent regimes, the humped shape of the PDF indicates larger frequency of events contributing to streamflow as compared to the recession time scale with reduced flow variability. In contrast, in erratic regimes the monotonically decreasing shape of the PDF signifies smaller frequency of flow-producing events and enhanced flow variability. In Daddy Creek, there is a shift in streamflow PDF from hump-shaped in spring and winter seasons to monotonically decreasing in summer and autumn seasons (Figure 7). This is consistent with rainfall and PET patterns across the seasons (see *Botter,* [2014]).

The insets of Figure 7 present the observed (circles) and modeled (solid line) CDFs of all seasons at Daddy Creek. A logarithmic scale has been used in order to better represent the behavior of the curves for large streamflows. The modeled CDFs are slightly shifted downward as compared to the observed CDFs. This is as a result of

the reduced amount of water available for streamflow generation estimated by the water balance model. Nevertheless, the shape of the CDF seems to be reasonably captured in most seasons.

Figure 8 shows the the observed (bars) and modeled (solid line) PDFs for the summer season at the five other test catchments. During the summer season an erratic regime is observed as a result of low rainfall and enhanced transpiration rates, which imply increased frequency of the smallest discharge events. The analytical model reasonably captures the shape of the streamflow PDFs in all cases. The associated modeled CDFs (The insets of Figure 8) show a similar behavior as discussed above.

The ability of the model to suitably mirror the observed intra-seasonal streamflow variability have been further analyzed through the mean ($\langle Q \rangle$) and coefficient of variation of daily discharge (CV_Q). Figure 9 shows the seasonal (a) $\langle Q \rangle$ and (b) CV_Q observed at all catchments plotted against the corresponding modeled values. The model estimates of both ($\langle Q \rangle$) and CV_Q have been computed through numerical integration of equation (2). In most cases prediction of the analytical model matches the corresponding observed CV_Q (MSRE = 0.06). This points to the models ability to reasonably capture the streamflow variability and its inter-seasonal dynamics across different climatic and landscape settings. The value of MSRE of mean discharge ($< Q >$) when all seasons at the eleven test catchments are considered is equal to 0.13.

6. Discussion

The framework presented here is structurally able to provide a reasonable estimation of streamflow regime based on limited information about climate and landscape. However, it should be noted that the stochastic streamflow model presented in this paper is best suited to describe flow regimes of pristine catchments with a contributing area smaller than a few thousand square kilometers, where streamflow dynamics result from the interaction between intermittent precipitation inputs and soil drainage. Although extensions to different settings (such as snow-dominated, urbanized or seasonally dry catchments) have been proposed [*Schaefli et al.,* 2013; *Müller et al.,* 2014; *Mejia et al.,* 2014], their predictive power in the absence of discharge measurements must be assessed. Moreover, the estimate of the model parameters based on climate and landscape requires

the introduction of additional assumptions and parameters that may reduce the accuracy of the flow regime predictions. In the set of cases explored here, model performances were satisfactory, but more research is recommended to explore the reliability of the approach in a wider array of case studies.

The accuracy of the estimate of a (i.e. the degree of non-linearity of the hydrologic response) based on catchment morphology, is constrained by the resolution of DEM, the drainage density of the network, and its spatial patterns both within each catchment and among different basins [*Mutzner et al.,* 2013]. Moreover, the application to relatively flat catchments may be problematic due to lack of accuracy of automatically extracted networks and the dominant role played by hydrological features. An accurate estimation of the frequency of flow producing events (λ) may be challenging in presence of small-scale geologic heterogeneity. Also, the reliability of the water balance estimate is influenced by the type of model used. Our results suggest that suitably calibrated physically-based models perform better than empirical methods (such as Budyko), but require data from nearby sites or large-scale regional studies for their calibration. Where no information is available, empirical methods can be utilized, with increased uncertainty about the accuracy of the prediction. The estimation of α and K on the other hand is less precarious. The value of α is calculated from readily available long-term daily rainfall records, with limited uncertainty. The value of K is dependent on λ, α and a which makes the accuracy of its estimation dependent on the deviation of those parameters (Table 6). However, sensitivity of the analytical streamflow distribution to the parameter K is quite limited, particularly for values of a close to 2 [see *Botter et al.,* 2009]. This implies (and our result corroborate) that a rough estimate of the recession coefficient suffices for predicting $p(Q)$ with a reasonable accuracy.

@basudev: please write a a few short sentences on the applicability and performance of the model in very arid regions/dry conditions (summer seasons).

@gianluca: do you think we need to discuss the mass balance topic here? We could say that if carryover is negligible the effects are insignificant. When that is not the case, the model is not applicable (for example the case of snow dominated catchments mentioned previously). If we were to say carry over is negligible in the cases stuied, that would upset too many people. Alternatively, we could say we study the seasonal regimes,

and that not significant carryover is allowed/considered in the framework.

7. Conclusion

A framework is provided that allows for estimating the probability distribution of streamflows based on catchment scale climate and geomorphologic data. The approach employs a physically-based analytic model of streamflows with four parameters. It was shown that these parameters can be estimated in the absence of discharge time series, by exploiting climate data (precipitation, potential evapotranspiration) and information about the catchment morphology.

The estimation procedure required the use of additional models, which were taken from the existing literature. A geomorphologic flow recession model was utilized to estimate parameters describing the recession behavior of the hydrograph, based on the topology of the stream network. A water balance model was used to predict the frequency of flow producing rainfall events. As the latter proves particularly important to predict the flow regime at a station, four existing water balance models were tested using rainfall and discharge data from 38 US catchments, characterized by diverse hydro-climatological characteristics. The best performing model (according to the Akaike selection criterion) was then used for the prediction of seasonal streamflow regimes in a disjointed set of catchments within the considered study area.

The results demonstrated that the model is capable of capturing the statistics of streamflows reasonably well in most of the cases analyzed. The largest deviations from observations were associated to reduced performance of the water balance models, that at times failed to accurately reproduce the observed seasonal runoff coefficients.

Our results suggest that the method has the potential for estimating the probability density function of river flows based on limited (and widely available) information on climate and landscape. The framework has implications for a wide range of practical and scientific applications such as water resources management, ecological studies and flood risk assessment. Further efforts are needed to investigate the performance of the model in a wider array of catchments, and to test the applicability of the method in data-scarce regions. This is the objective of ongoing research.

Acknowledgments

The research leading to these results has received funding from the European Community's Seventh Framework Program (FP7/2007-2013 under grant agreement n265063). This study was also funded by the Swiss National Science Foundation (SNF, Projects No. 200021-149126). Additional support was provided by the Competence Center Environment and Sustainability (CCES) of the ETH domain in the framework of the RECORD and RECORD Catchment projects. Gianluca Botter acknowledges funding from project 60A09-4895/13 "Regimi idrologic e cambiamenti climatici". The EU project "SmartWater" is also acknowledged. Special thanks to i4 Consulting S.r.l. for their data management services.

References

[1] Akaike, H. (1974), A new look at the statistical model identification. *Trans. on Aut. Cont.*, 19 , 716-723, doi:10.1109/TAC.1974.1100705.

[2] Allen, R., L. S. Pereira, D. Raes, M. Smith (1998), Crop evapotranspiration - Guidelines for computing crop water requirements, *FAO Irrigation and Drainage Paper*, 56, FAO, Rome.

[3] Beven, K.J. and Kirkby, M.J. (1979), A physically based, variable contributing area model of basin hydrology. *Hydro. Sci. Bull.*, 24, 4369. doi:10.1080/02626667909491834.

[4] Biondi, D., G. Freni, V. Iacobellis, G. Mascaro, A. Montanari (2012), Validation of hydrological models: Conceptual basis, methodological approaches and a proposal for a code of practice, *Phy. Chem. Earth*, doi:10.1016/j.pce.2011.07.037.

[5] Biswal, B., and M. Marani (2010), Geomorphological origin of recession curves, *Geo. Res. Letters* 37, doi:10.1029/2010GL045415.

[6] Biswal, B., D. Nagesh Kumar (2013), A general geomorphological recession flow model for river basins, *Water. Resour. Res*, 49, doi:10.1002/wrcr.20379.

[7] Biswal, B., D. Nagesh Kumar (2014), What mainly controls recession flows in river basins?, *Adv. Water Res.*, 65, 25-33, doi:10.1016/j.advwatres.2014.01.001.

[8] Biswal, B., and M. Marani (2014), Universal recession curves and their geomorphological interpretation, *Adv. Water Res.*, doi:10.1016/j.advwatres.2014.01.004.

[9] Booker, D. J., R. A. Woods (2014), Comparing and combining physically-based and empirically-based approaches for estimating the hydrology of ungauged catchments, *J. Hydro.*, doi:10.1016/j.jhydrol.2013.11.007.

[10] Botter, G., A. Porporato, I. Rodriguez-Iturbe, A. Rinaldo (2007), Basin-scale soil moisture dynamics and the probabilistic characterization of carrier hydrologic flows: Slow, leaching-prone components of the hydrologic response, *Water. Resour. Res* 43, doi:10.1029/2006WR005043.

[11] Botter, G., S. Zanardo, A. Porporato, I. Rodriguez-Iturbe, A. Rinaldo (2008), Ecohydrological model of flow duration curves and annual minima. *Water. Resour. Res* 44, doi:10.1029/2008WR006814.

[12] Botter, G., A. Porporato, I. Rodriguez-Iturbe, A. Rinaldo (2009), Nonlinear storage-discharge relations and catchment streamflow regimes, *Water. Resour. Res* 45, doi:10.1029/2008WR007658.

[13] Botter, G., S. Basso, I. Rodriguez-Iturbe, and A. Rinaldo (2013), Resilience of river flow regimes, *Proc. Natl. Acad. Sci.*, doi:10.1073/pnas.1311920110.

[14] Botter, G., Flow regime shifts in the Little Piney creek (US), *Adv. Water Res.*, doi:10.1016/j.advwatres.2014.05.010.

[15] Blöschl G., Rainfall-runoff modeling of ungauged catchments (2006), *Encyclopedia of Hydrological Sciences*, NJ: Wiley, doi:10.1002/0470848944;

[16] Brutsaert, W., and J. L. Nieber (1977), Regionalized drought flow hydrographs from a mature glaciated plateau, *Water. Resour. Res* 13(3), 637-644, doi:10.1029/WR013i003p00637.

[17] Budyko, M. I. (1974), Climate and life. *Academic*, San Diego, California, 508 pp.

[18] Castellarin, A., R.M. Vogel, A. Brath (2004), A stochastic index flow model of flow duration curves. *Water. Resour. Res*, 40, W03104, doi:10.1029/2003WR002524.

[19] Castellarin, A., G. Camorani, A. Brath (2007), Predicting annual and long-term flow-duration curves in ungauged basins, *Adv. Water Res.*, 30, 937-953, doi:10.1016/j.advwatres.2006.08.006.

[20] Castiglioni, S., L. Lombardi, E. Toth, A. Castellarin, A. Montanari (2010), Calibration of rainfall-runoff models in ungauged basins: A regional maximum likelihood approach, *Adv. Water. Res.*, doi: 10.1016/j.advwatres.2010.04.009

[21] Ceola, S., G. Botter, E. Bertuzzo, A. Porporato, I. Rodriguez-Iturbe, A. Rinaldo (2010), Comparative study of ecohydrological streamflow probability distributions, *Water. Resour. Res*, 46, W09502, doi:10.1029/2010WR009102.

[22] Cheng, L., et al., 2012. Exploring the physical controls of regional patterns of flow duration curves-part 1: insights from statistical analyses, *Hydro. Earth Sys. Sci.*, 16, 44354446, doi:10.5194/hess-16-4435-2012.

[23] Destouni, G., F. Jaramillo, C. Prieto (2013), Hydroclimatic shifts driven by human water use for food and energy production, *Nat. Cli. Change*, doi:10.1038/NCLIMATE1719.

[24] Donohue, R. J., M. L. Roderick, and T. R. McVicar (2007), On the importance of including vegetation dynamics in Budyko's hydrological model, *Hydrol. Earth Syst. Sci.*, 11(2), 983995, doi:10.5194/hess-11-983-2007.

[25] Ganora, D., P. Claps, F. Laio, A. Viglione (2009), An approach to estimate nonparametric flow duration curves in ungauged basins. *Water. Resour. Res*, 45:W10418. doi:10.1029/2008WR007472.

[26] Gregory, K. J., and D. E. Walling (1968), The variation of drainage density within a catchment, *Bull. Intn. Ass. Sci. Hydr.*, 13(2), 6168, doi:10.1080/02626666809493583.

[27] Godsey, S. E. and J. W. Kirchner (2014), Dynamic, discontinuous stream networks: hydrologically driven variations in active drainage density, flowing channels and stream order, *Hydr. Proc.*, doi: 10.1002/hyp.10310

[28] Gupta, H. V., T. Wagener, Y. Liu (2008), Reconciling theory with observations: elements of a diagnostic approach to model evaluation. Hydrological Processes, 22, 38023813, *Hydr. Proc.*, doi:10.1002/hyp.6989.

[29] Harman, C., and M. Sivapalan (2009), A similarity framework to assess controls on shallow subsurface flow dynamics in hillslopes, *Water. Resour. Res*, 45, W01417, doi:10.1029/2008WR007067.

[30] Hrachowitz, M., H. H. Savenije, G. Blöschl, J. J. McDonnell, M. Sivapalan, J. Pomeroy, B. Arheimer, T. Blume, M. P. Clark, U. Ehret, F. Fenicia, J.E. Freer, A. Gelfan, H.V. Gupta, D.A. Hughes, R.W. Hut, A. Montanari, S. Pande, D. Tetzlaff, P.A. Troch, S. Uhlenbrook, T. Wagener, H.C.Winsemius, R.A.Woods, E. Zehe, C. Cudennec (2013), A decade of Predictions in Ungauged Basins (PUB) a review (2013), *Hydrolog. Sci. J.*, doi:10.1080/02626667.2013.803183.

[31] Hurford, A. P. and J. J. Harou (2014), Balancing ecosystem services with energy and food security-Assessing trade-offs from reservoir operation and irrigation investments in Kenyas Tana Basin, *Hydrol. Earth Syst. Sci.*, 18, 32593277, doi:10.5194/hess-18-3259-2014.

[32] Kirchner, J. W. (2009), Catchments as simple dynamical systems: Catchment characterization, rainfall-runoff modeling, and doing hydrology backward, *Water. Resour. Res*, 45, W02429, doi:10.1029/2008WR006912.

[33] Langbein, W.B. (1949), Annual runoff in the United States, *Geol. Surv. Circ.*, 52 (1949) 14

[34] L'vovich, M. I. (1979), World Water Resources and Their Future, pp 415.

[35] Mark, D. M. (1988), Network models in geomorphology, Chapter 4 in *Model. Geomorph. Sys.*, Edited by M. G. Anderson, John Wiley, 73-97.

[36] Mejia, A., E.Daly, F. Rossel, T. Jovanovic, J. Gironas (2014), A stochastic model of streamflow for urbanized basins, *Water. Resour. Res*, doi:10.1002/2013WR014834.

[37] Merz, R., and G. Blschl, (2004), Regionalisation of catchment model parameters. *Jour. Hydro.*, 287, 95123, doi:10.1016/j.jhydrol.2003.09.028

[38] Milly, P. C. D. (1994), Climate, iterseasonal storage of soil water, and the annual water balance, *Adv. Water Resour.*.

[39] Müller M. F., D. N. Dralle, S. E. Thompson (2014), Analytical model for flow duration curves in seasonally dry climates, *Adv. Water Res.*, doi:10.1002/2014WR015301.

[40] Mutzner R, E. Bertuzzo, P. Tarolli, S. V. Weijs, L. Nicotina, S. Ceola, N. Tomasic, I. Rodriguez-Iturbe, M. B. Parlange, A. Rinaldo (2013), Geomorphic signatures on Brutsaert base flow recession analysis, *Water. Resour. Res*, 49:546272. doi:10.1002/wrcr.20417.

[41] Oudin, L., V. Andreassian, C. Perrin, C. Michel, N. Le Moine (2008), Spatial proximity, physical similarity, regression and ungagged catchments: a comparison of regionalization approaches based on 913 French catchments, *Water. Resour. Res*, 44, W03413, doi:10.1029/2007WR006240.

[42] Ponce, V. M., and A. V. Shetty, (1995a), A conceptual model of catchment water balance: 1. Formulation and calibration, *Jour. hydr.* 173, 27-40, doi:10.1016/0022-1694(95)02739-C.

[43] Ponce, V. M., and A. V. Shetty, (1995b), A conceptual model of catchment water balance: 2. Application to runoff and baseflow modeling, *Jour. hydr.* 173, 4150, doi:10.1016/0022-1694(95)02745-B.

[44] Porporato, A., and L. Ridolfi (2003), Detecting determinism and nonlinearity in river-flow time

series, *Hydr. Sci. Jour.*, vol 48 no. 5 , pp. 763-780, doi:10.1623/hysj.48.5.763.51457.

[45] Porporato, A., E. Daly, I. Rodriguez-Iturbe, (2004), Soil water balance and ecosystem response to climate change, *Am. Nat.*, 164, doi:10.1086/424970.

[46] Postel, S., and B. Richter (2003), Rivers for Life: Managing Water for People and Nature, *Island Press*, Washington, DC.

[47] Rinaldo, A. (1991), Geomorphological Dispersion, *Water Resour. Res.*, VOL. 27, NO. 4, PAGES 513-525, doi:10.1029/90WR02501.

[48] Rinaldo, A., G.K. Vogel, R. Rigon, I. RodriguezIturbe (1995), Can one gauge the shape of a basin?, *Water. Resour. Res.*, doi: 10.1029/95WR03290.

[49] Rodriguez-Iturbe, I., A. Porporato, L. Ridolfi, V. Isham, D. R. Coxi, (1999), Probabilistic modelling of water balance at a point: the role of climate, soil and vegetation, *Proc. Royal Soc. London*, doi:10.1098/rspa.1999.0477.

[50] Rodriguez-Iturbe I, A. Porporato, F. Laio, L. Ridolfi (2001), Plants in water-controlled ecosystems: active role in hydrologic processes and response to water stress I. Scope and general outline, *Adv. Water Resour.*, doi:10.1016/s0309-1708(01)00004-5.

[51] Rodriguez-Iturbe, I., R. Muneepeerakul, E. Bertuzzo, S. A. Levin, and A. Rinaldo (2009), River networks as ecological corridors: A complex systems perspective for integrating hydrologic, geomorphologic, and ecologic dynamics, *Water Resour. Res.*, 45, W01413, doi:10.1029/2008WR007124.

[52] Schaefli, B., A. Rinaldo, G. Botter (2013), Analytic probability distributions for snow-dominated streamflow, *Water Resour. Res.*, doi:10.1002/wrcr.2023.

[53] Sivapalan, M., M. A. Yaeger, C. J. Harman, X. Xu, P. A. Troch, (2011), Functional model of water balance variability and the catchment scale: 1. Evidence of hydrologic similarity and space-time symmetry, *Water Resour. Res.*, 47, doi:10.1029/2010WR009568.

[54] Thompson, S. E., C. J. Harman, A. G. Konings, M. Sivapalan, A. Neal, P. A. Troch (2011a), Comparative hydrology across AmeriFlux sites: The variable roles of climate, vegetation, and groundwater, *Water Resour. Res.*, 47, W00J07, doi:10.1029/2010WR009797.

[55] Thompson, S. E., C. J. Harman, P. A. Troch, P. D. Brooks, M. Sivapalan (2011b), Spatial scale dependence of ecohydrologically mediated water balance partitioning: A synthesis framework for catchment ecohydrology, *Water Resour. Res.* 47, W00J03, doi:10.1029/2010WR009998.

[56] Thorntwaite, C.W., (1948), An approach toward a rational classification of climate,*Geog. Review*, 94(1948) 38-55.

[57] Troch, P. A., G. F. Martinez, V. R. N. Pauwels, M. Durcik, M. Sivapalan, C. Harman, P. D. Brooks, H. Gupta, T. Huxman (2009), Climate and vegetation water use efficiency at catchment scales, *Hydrol. Process.*, 23(16), 24092414, doi:10.1002/hyp.7358.

[58] Pumo, D., L.V. Noto, F. Viola (2013), Ecohydrological modelling of flow duration curve in Mediterranean river basins,*Adv. Water Resour.*, 52:31427, doi:10.1016/j.advwatres.2012.05.010.

[59] Voepel, H., B. Ruddell, R. Schumer, P. A. Troch, P. D. Brooks, A. Neal, M. Durcik, M. Sivapalan (2011), Quantifying the role of climate and landscape characteristics on hydrologic partitioning and vegetation response, *Water Resour. Res.*, doi:10.1029/2010WR009944.

[60] Vogel, R. M., and N. M. Fennessey (1995), Flow duration curves II : A review of applications in water resources planning, *J. Am. Water Resour. Assoc.*, 31(6), 10291039, doi:10.1111/j.1752-1688.1995.tb03419.

[61] Wagener, T., M. Sivapalan, P. Troch, R. Woods (2007), Catchment classification and hydrologic similarity. *Geography Compass*, 1 (4), 901931, doi:10.1111/j.1749-8198.2007.00039.x.

[62] Wagener, T., H.S. Wheater, and H.V. Gupta (2004), Rainfallrunoff modeling in gauged and ungauged catchments. *Imperial College Press*, London.

[63] Weyman, D. R. (1970), Throughflow in hillslopes and its relation to stream hydrograph, *Bul. Int. Ass. Sci. Hydr.*, 15(3), 25-33, doi:10.1080/02626667009493969.

[64] Yokoo, Y., and M. Sivapalan (2011), Towards reconstruction of the flow duration curve: development of a conceptual framework with a physical basis, *Hydr. Earth Sys. Sci.*, 15, 2805-2819, doi:10.5194/hess-15-2805-2011.

[65] Ziva, G., E. Baranb, S. Nam, I. Rodriguez-Iturbe, and A. L. Simon (2012), Trading-off fish biodiversity, food security, and hydropower in the Mekong River Basin, *Proc. Natl. Acad. Sci*, 56095614, doi:10.1073/pnas.120142310.

[66] Zhang, L., N. Potter, K. Hickel, Y. Zhang, Q. Shao (2008), Water balance modeling over variable time scales based on the Budyko frameworkModel development and testing, *J. Hydrol.*, 360(14),117131, doi:10.1016/j.jhydrol.2008.07.021.

[67] Zanardo, S., C. Harman, P. A. Troch, S. C. Rao, and M. Sivapalan (2012), Intra-annual rainfall variability controls on inter-annual variability of catchment water balance: A stochastic analysis, *Water Resour. Res.*, 48(6), doi:10.1029/2010WR009869.

[68] Zomer, R. J., D. A. Bossio, A. Trabucco, L. Yuanjie, D. C. Gupta, V. P. Singh (2007), Trees and water: smallholder agroforestry of irrigated lands in northern India, *Colombo, Sri Lanka: International water management institute*, pp. 45, doi:10.3910/2009.122.

Table 1: Summary information about the 38 catchments used for the calibration.

	USGS Code	Catchment	Area [km^2]	Streamflow Gauging Station	Rainfall Gauging Station	State	Period
1	02316000	Alapaha River	1717	Alapaha	Alapaha Exp Stn	GA	1951-2013
2	05399500	Big Eau Pleine River	580	Stratford	Stratford 1NW	WI	1950-2013
3	06893100	Blue River	170	Kenneth	Stilwell	KS	2003-2013
4	07261000	Cadron Creek	438	Guy	Greenbrier	AR	1961-2013
5	03419800	Calfkiller River	453	Sparta	Sparta Waste Water Plan	TN	2003-2013
6	07172000	Caney River	1153	Elgin	Cedar Vale 5 SSE	KS	1961-2013
7	07021000	Castor River	1090	Zalma	Zalma 4E	MO	1951-2013
8	03539778	Clear Creek	440	Lancing	Lancing 6 NW	TN	1999-2013
9	02380500	Coosawattee River	611	Ellijay	Ellijay	GA	1951-2013
10	08101000	Cowhouse Creek	1167	Pidkoke	Pidcoke	TX	1976-2013
11	02133500	Drowning Creek	474	Hoffman	Jackson Springs 5 WNW	NC	1954-2013
12	02326000	Econfina River	513	Perry	Perry	FLA	1957-2013
13	01170100	Green River	107	Colrain	Whitingham	MA	1969-2013
14	02143500	Indian Creek	179	Laboratory	Lincoln 4 W	NC	1952-2013
15	02143040	Jakob Fork	67	Ramsey	Casar	ND	1961-2013
16	06339100	Knife River	531	Manning	Fairfield	ND	1971-2013
17	01057000	Little Androscoggin River	190	South Paris	West Paris	ME	1980-2013
18	03109500	Little Beaver Creek	1284	East Liverpool	Millport 3NE	OH	1951-2013
19	07346070	Little Cypress Bayou	1748	Jefferson	Harleton	TX	1951-2013
20	03438000	Little River	632	Cadiz	Hopkinsville	KY	1951-2013
21	04270200	Little Salmon River	239	Bombay	Malone	NY	1985-2013
22	03216500	Little Sandy River	1036	Grayson	Grayson 3 SW	KY	1951-2013
23	06478540	Little Vermillion River	204	Salem	Montrose	SD	1968-2013
24	04115000	Maple River	1124	Maple Rapids	Saint Johns	MI	1951-2013
25	08189500	Mission River	1787	Refugio	Beeville 5 NE	TX	1987-2013
26	03326500	Mississinewa River	1766	Marion	Marion 2 N	IN	1951-2013
27	07144780	Nf Ninnescah River	1847	Caheny	Hutchinson 10 SW	KS	1984-2013
28	03346000	North Fork Embarras River	824	Oblong	Casey	IL	1951-2013
29	08160800	Redgate Creek	45	Columbus	Columbus	TX	1964-2013
30	02034000	Rivanna River	1717	Palmyra	Charlottesville 2 W	VA	1951-2013
31	05060500	Rush River	300	Amenia	Casselton Agronomy	ND	1986-2013
32	06803000	Salt Creek	433	Roca	Roca	NE	1953-2013
33	07185765	Spring River	1101	Carthage	Mt Vernon	MO	1968-2013
34	07375500	Tangipahoa River	1673	Robert	Hammond 5 W	GA	1981-2013
35	01518000	Tioga River	730	Tioga	Covington 2 WSW	GA	1958-2013
36	02462000	Valley Creek	383	Oak Grove	Bankhead Dam	GA	1959-2013
37	01343060	West Canada Creek	668	Wilmurt	Piseco	NY	2003-2013
38	06444000	White River	811	Crawford	Ft Robinson	NE	1941-2013

Table 2: Summary information about the 11 test catchments.

	USGS Code	Catchment	Area [km^2]	Streamflow Gauging Station	Rainfall Gauging Station	State	Period
A	03075500	Youghiogheny River	347	Oakland	Oakland 1 SE	MD	1951-2013
B	03539600	Daddys Creek	360	Hebbertsburg	Crossville mep ap	TN	1958-2013
C	07257006	Big Piney Creek	793	Highway 164	Deer	AR	1995-2013
D	03052500	Sand Run	37	Buckhannon	Buckhannon	WV	1951-2013
E	07015720	Bourbeuse River	350	High Gate	vichy rolla	MO	1966-2014
F	03368000	Brush Creek	30	Nebraska	north vernon	IN	1956-2014
G	07260000	Dutch creek	211	Waltreak	gravelly	AR	1946-2014
H	07335700	Kiamichi River	103	Big Cedar	mena	OK	1966-2014
I	02384540	Mill creek	21	Crandall	chatsworth	GA	1986-2014
J	02450250	Sipsey Fork	239	Grayson	haleyville	AL	1967-2014
K	03211500	Johns Creek	534	Van Lear	fishtrap lake	KY	1970-2014

Table 3: Water balance models.

Code	Relevant References	Type	Number of parameters
WB1	Budyko, 1974	Empirical	0
WB2	Porporato et al., 2004	Physically-based	1-4
WB3	P.C.D. Milly, 1994	Physically-based	2
WB4	Sivapalan et al., 2011	Functional	4

Table 4: Ranking of water balance models applied at the annual time scale.

Rank	Model	Δ AIC	MSE	Number of parameters	Parameters
1	WB4.ET1.A	0.0	0.0079	1	$\lambda_u = 0.2$
2	WB4.ET2.A	8.0	0.0097	1	$\lambda_u = 0.2$
3	WB1.ET1.A	11.6	0.0112	0	-
4	WB2.ET1.A	16.6	0.0121	1	$Z = 420mm$
5	WB2.ET2.A	26.8	0.0157	1	$Z = 300mm$
6	WB3.ET1.A	29.8	0.0161	2	$Z = 900mm$, $k = 0.525$
7	WB1.ET2.A	36.9	0.0214	0	-
8	WB3.ET2.A	38.8	0.0203	2	$Z = 700mm$, $k = 0.525$

Table 5: Ranking of water balance models applied at the seasonal time scale. Subscripts of Z indicate the different seasons (sp = spring, su = summer, au = autumn, and wi = winter).

Rank	**Model**	**Δ AIC**	**MSE**	**Number of parameters**	**Parameters**
1	WB2.ET2.S	0	0.0133	4	$Z_{wi} = 570mm$, $Z_{sp} = 195mm$, $Z_{su} = 510mm$, $Z_{au} = 975mm$
2	WB2.ET1.S	1.0	0.0134	4	$Z_{win} = 1500mm$, $Z_{sp} = 240mm$, $Z_{su} = 570mm$, $Z_{au} = 1500mm$
3	WB2.ET1.Sc	11.7	0.0142	4	$Z = 420mm$, $\psi_{wi} = 1.44$, $\psi_{sp} = 1.42$, $\psi_{su} = 0.56$, $\psi_{au} = 0.59$
4	WB2.ET1.S	21.6	0.0161	2	$Z_{su,sp} = 450mm$, $Z_{au,wi} = 1500mm$
5	WB2.ET2.S	34.3	0.0177	2	$Z_{su,sp} = 330mm$, $Z_{au,wi} = 900mm$
6	WB2.ET2.Sc	41.1	0.0184	5	$Z = 300mm$, $\psi_{wi} = 1.44$, $\psi_{sp} = 1.42$, $\psi_{su} = 0.56$, $\psi_{au} = 0.59$
7	WB3.ET1.Sc	43.8	0.0186	6	$Z = 300mm$, $k = 0.0525$, $\psi_{wi} = 1.44$, $\psi_{sp} = 1.42$, $\psi_{su} = 0.56$, $\psi_{au} = 0.59$
8	WB2.ET2.S	60.8	0.0219	1	$Z = 435mm$
9	WB1.ET2.S	63.0	0.0226	0	-
10	WB3.ET2.Sc	66.5	0.0215	6	$Z = 700mm$, $k = 0.0525$, $\psi_{wi} = 1.44$, $\psi_{sp} = 1.42$, $\psi_{su} = 0.56$, $\psi_{au} = 0.59$
11	WB1.ET1.S	66.6	0.0232	0	-
12	WB2.ET1.S	68.0	0.0231	1	$Z = 615mm$
13	WB1.ET1.Sc	100.7	0.0281	4	-
14	WB4.ET1.Sc	103.7	0.0271	5	$\lambda_u = 0.2$, $\psi_{wi} = 1.44$, $\psi_{sp} = 1.42$, $\psi_{su} = 0.56$, $\psi_{au} = 0.59$
15	WB4.ET2.Sc	109.7	0.0300	5	$\lambda_u = 0.2$, $\psi_{wi} = 1.44$, $\psi_{sp} = 1.42$, $\psi_{su} = 0.56$, $\psi_{au} = 0.59$
16	WB1.ET2.Sc	134.9	0.0367	4	-

Table 6: Estimated value of model parameters for all seasons at the eleven test catchments.

Catchment Name	Season	Estimated from Climate and Geomorphologic Data				Estimated from Discharge Data		
		$\alpha[cm]$	$\lambda[\frac{1}{d}]$	$K[\frac{cm^{(1-a)}}{d^{(2-a)}}]$	$a[-]$	$\lambda[\frac{1}{d}]$	$K[\frac{cm^{(1-a)}}{d^{(2-a)}}]$	$a[-]$
Youghiogheny River (A)	*Spring*	0.73	0.19	0.84	1.65	0.45	0.45	1.68
	Summer	0.89	0.07	1.48	1.65	0.13	1.09	1.75
	Autumn	0.74	0.09	1.30	1.65	0.15	1.27	1.90
	Winter	0.63	0.35	0.62	1.65	0.50	0.57	1.84
Daddy Creek (B)	*Spring*	1.08	0.18	0.87	1.81	0.26	0.61	1.73
	Summer	1.02	0.06	2.31	1.81	0.05	1.05	1.44
	Autumn	1.04	0.07	1.91	1.81	0.07	1.42	1.67
	Winter	0.95	0.26	0.71	1.81	0.31	0.71	1.89
Big Piney Creek (C)	*Spring*	1.61	0.16	1.16	2.19	0.17	0.45	1.57
	Summer	1.17	0.03	9.75	2.19	0.04	0.92	1.54
	Autumn	1.79	0.10	1.99	2.19	0.04	1.25	1.71
	Winter	1.31	0.14	1.68	2.19	0.14	0.57	1.71
Sand Run River (D)	*Spring*	0.72	0.18	1.85	2.02	0.38	0.76	1.73
	Summer	0.95	0.07	3.79	2.02	0.09	1.43	1.52
	Autumn	0.76	0.08	3.84	2.02	0.12	1.86	1.76
	Winter	0.56	0.35	1.19	2.02	0.51	0.93	1.86
Bourbeuse River (E)	*Spring*	0.99	0.14	1.40	1.90	0.17	2.01	1.76
	Summer	1.17	0.04	1.20	1.90	0.05	1.98	1.47
	Autumn	1.11	0.05	3.81	1.90	0.05	2.78	1.76
	Winter	0.72	0.09	2.77	1.90	0.16	2.16	1.86
Brush Creek (F)	*Spring*	1.03	0.15	1.74	2.10	0.2	2.91	1.96
	Summer	1.17	0.05	5.20	2.10	0.05	3.95	1.63
	Autumn	1.00	0.05	5.89	2.10	0.05	8.41	1.92
	Winter	0.84	0.18	1.86	2.10	0.20	2.63	1.87
Dutch Creek (G)	*Spring*	1.51	0.14	1.36	2.15	0.14	1.07	1.78
	Summer	1.33	0.04	7.47	2.15	0.02	1.11	1.47
	Autumn	1.57	0.06	3.41	2.15	0.03	1.46	1.67
	Winter	1.26	0.13	1.80	2.15	0.12	0.96	1.76
Kiamichi River (H)	*Spring*	1.45	0.17	0.74	1.85	0.22	0.49	1.58
	Summer	1.21	0.04	2.86	1.85	0.06	0.56	1.26
	Autumn	1.56	0.11	1.05	1.85	0.09	0.76	1.51
	Winter	1.14	0.17	0.93	1.85	0.23	0.47	1.67
Mill Creek (I)	*Spring*	1.18	0.14	3.28	2.50	0.23	0.85	2.22
	Summer	1.10	0.06	12.06	2.50	0.10	1.19	2.00
	Autumn	1.30	0.07	8.00	2.50	0.10	2.92	2.23
	Winter	1.10	0.22	1.84	2.50	0.29	0.82	2.14
Sipsey Fork (J)	*Spring*	1.58	0.16	0.77	1.90	0.17	0.75	1.84
	Summer	1.28	0.06	2.21	1.90	0.04	3.10	1.85
	Autumn	1.47	0.08	1.49	1.90	0.04	5.46	2.03
	Winter	1.47	0.22	0.63	1.90	0.20	0.77	1.89
Johns Creek (K)	*Spring*	0.82	0.16	2.96	2.25	0.21	0.59	1.58
	Summer	0.96	0.06	8.53	2.25	0.05	1.34	1.53
	Autumn	0.87	0.07	7.90	2.25	0.08	0.42	1.54
	Winter	0.60	0.24	2.55	2.25	0.30	0.31	1.20

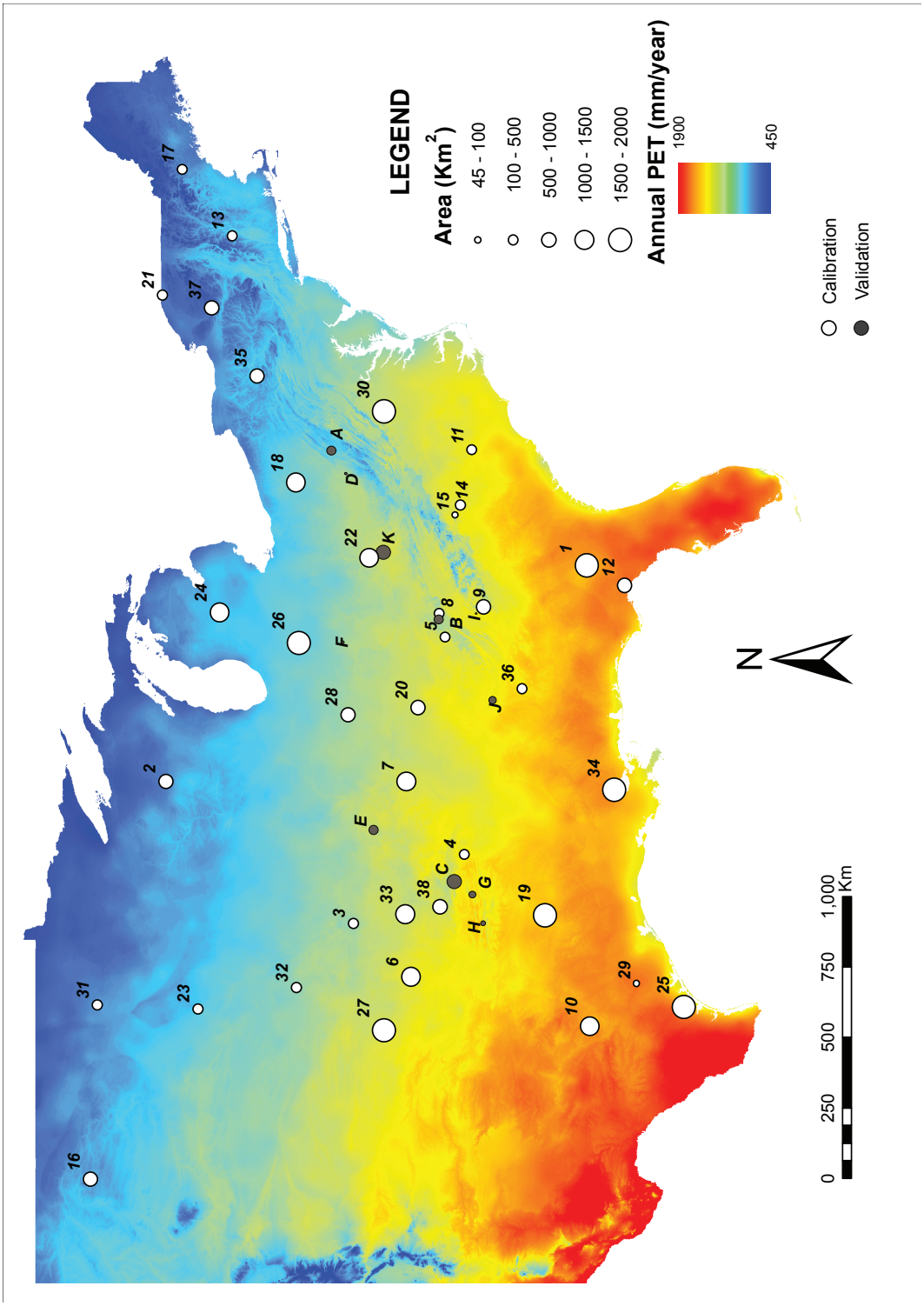

31

Figure 1: Spatial distribution of the 38 catchments used for the calibration of the water balance models and 11 test catchments (A through K) used for the prediction of the flow regime. On the background the *CGIAR* average annual potential evapotranspiration is shown to represent the underlying heterogeneity of climate regimes. The approximate size of each catchment is also depicted. The catchments marked with a dotted circle experience relevant snow precipitations during winter.

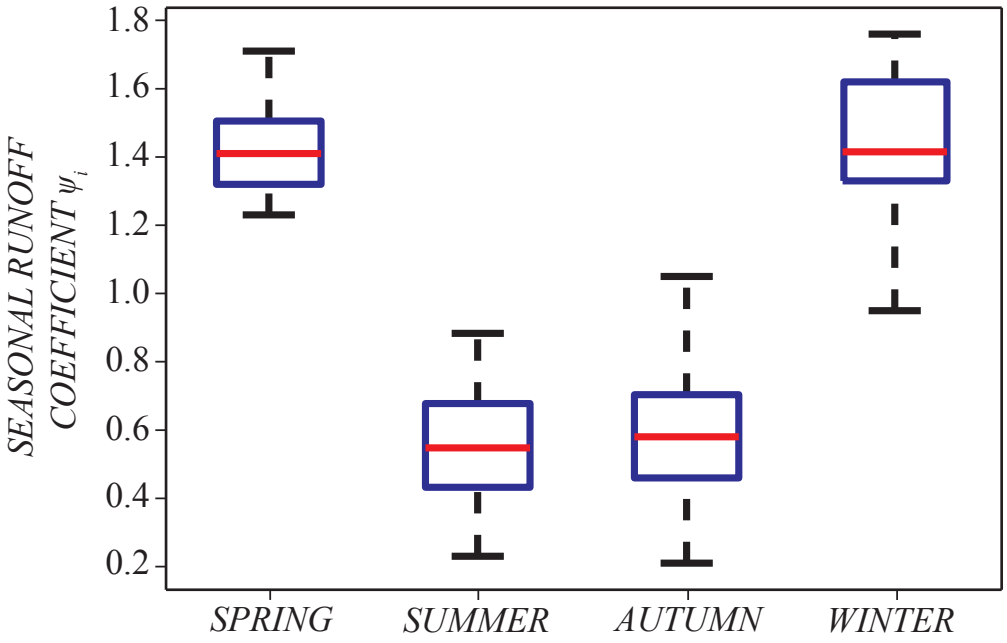

Figure 2: Seasonal multiplication factors for the four seasons: Spring (March, April, May), Summer (June, July, August), Autumn (September, October, November), Winter (December, January, February). The box plot shows the 25%, 50% and 75% quantiles as well as the entire range of observed values across the 38 study catchments.

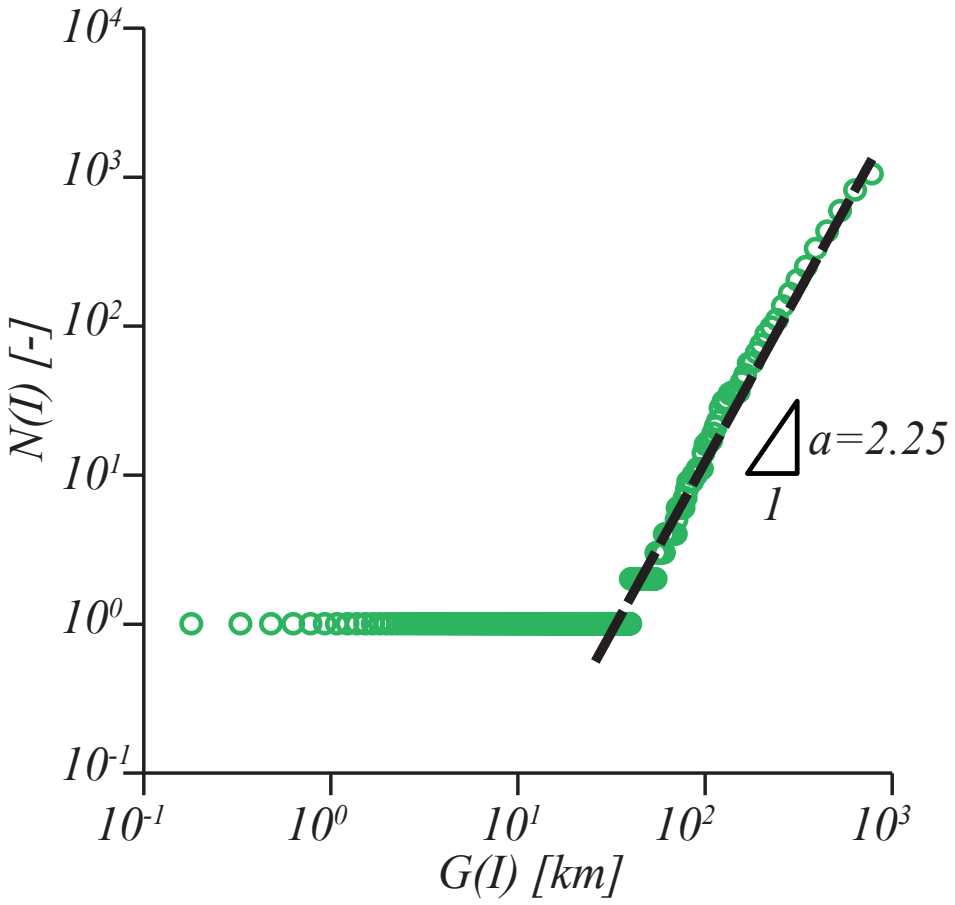

Figure 3: The recession exponent a is estimated from the morphology of the basin by analyzing the scaling exponent of the geomorphic relationship between $N(l)$ and $G(l)$.

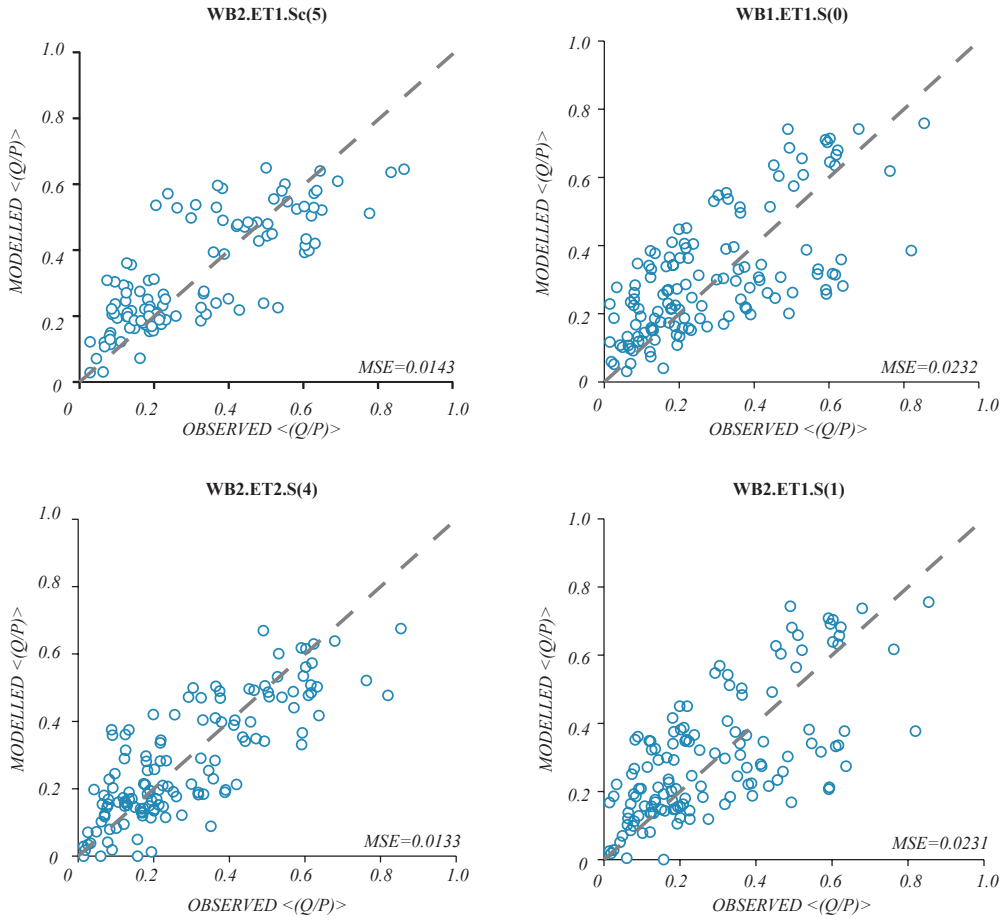

Figure 4: Scatter-plots of observed vs. estimated runoff coefficients by a select number of calibrated models at the seasonal time scale. The value of MSE is also included.

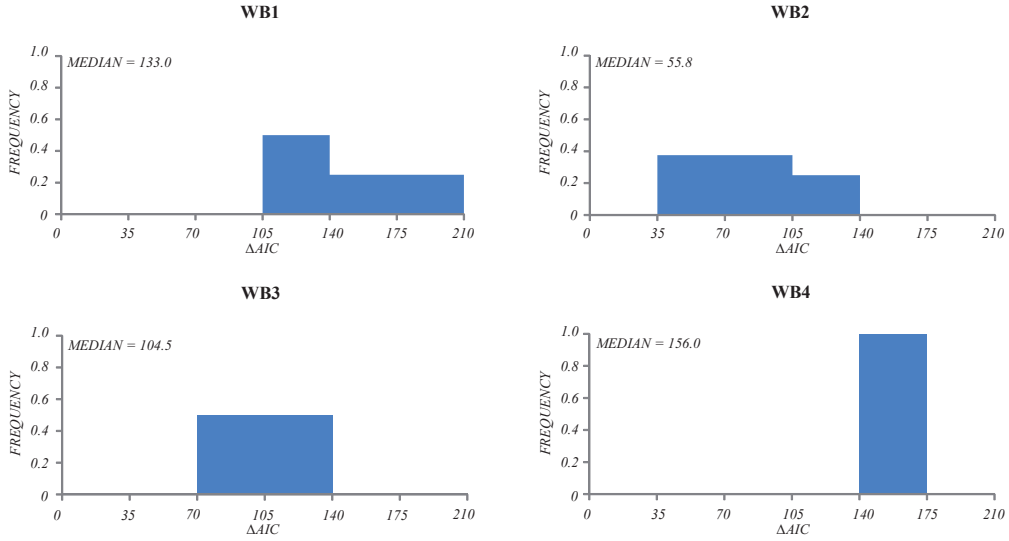

Figure 5: Frequency distribution of ΔAIC for all water balance models. The median value of ΔAIC is also included.

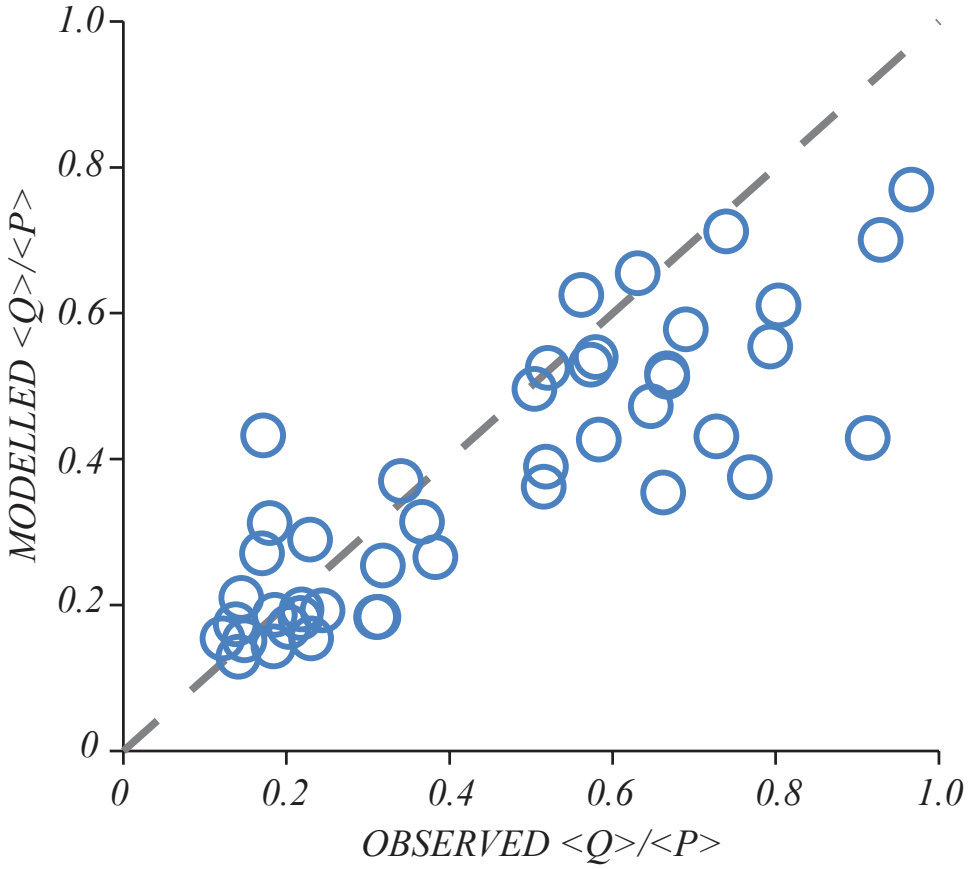

Figure 6: Scatter-plot of the seasonal average runoff coefficient for the eleven test catchments based on WB2.ET2.S(4) water balance model.

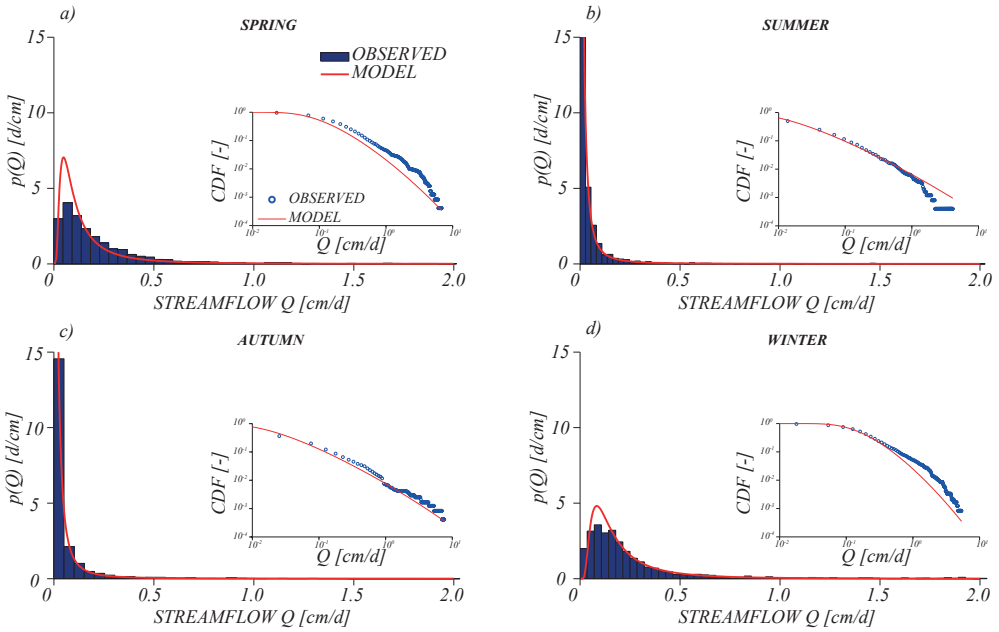

Figure 7: Observed (circles and bars) and modeled (solid line) PDFs and CDFs for (a) spring, (b) summer, (c) autumn and (d) winter at Daddy Creek, US. The integral difference between modeled and observed PDFs is equal to (a) 0.220, (b) 0.212, (c) 0.203, and (d) 0.163.

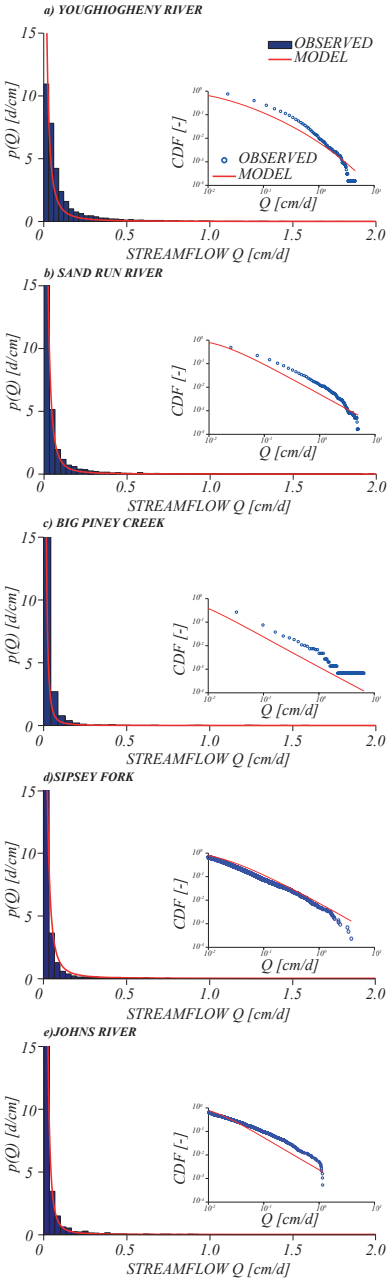

Figure 8: Observed (bars) and modeled (solid line) PDFs for summer season at (a) Youghiogheny River, US, (b) Sand Run River, US, (c) and Piney River, US, (d) Sipsey Fork, US, (e) Bourbeuse River, US. The integral difference between modeled and observed PDFs is equal to (a) 0.190, (b) 0.232, (c) 0.048, (d) 0.225, and (e) 0.314. The insets show the associated observed (circles) and modeled (solid line) CDFs for each plots.

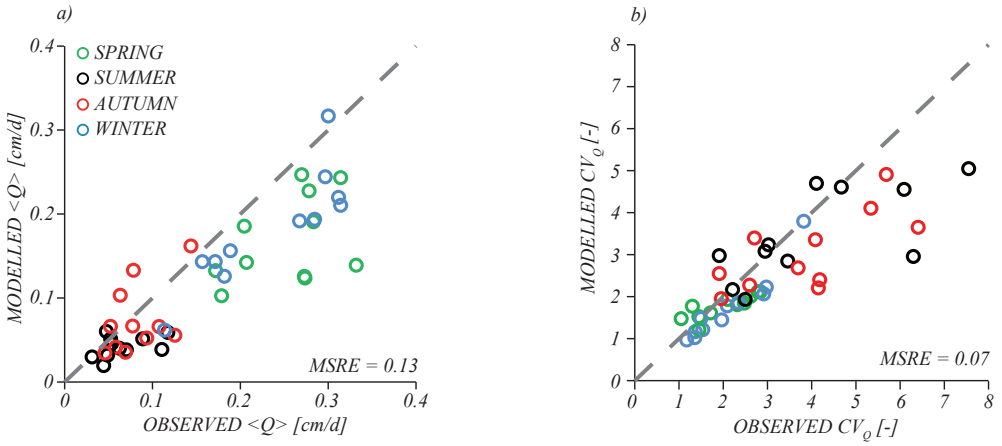

Figure 9: Observed vs. modeled (a) $\langle Q \rangle$ and (b) CV_Q for all seasons at the eleven considered test catchments. The dashed line represents the 45 degree line (perfect fit). The MSRE value associated with each variable is also mentioned in the figure.